THE JOURNAL OF PHYSICAL CHEMISTRY A

Subscriber access provided by BIU Pharmacie | Faculté de Pharmacie, Université Paris V

A: Spectroscopy, Molecular Structure, and Quantum Chemistry

3-Nitrene-2-Formylthiophene and 3-Nitrene-2-Formylfuran: Matrix-Isolation, Conformation, and Rearrangement Reactions

Jie Liu, Zhuang Wu, Yang Yang, Weiyu Qian, Lina Wang, and Xiaoqing Zeng

J. Phys. Chem. A, **Just Accepted Manuscript** • DOI: 10.1021/acs.jpca.9b11638 • Publication Date (Web): 20 Apr 2020

Downloaded from pubs.acs.org on April 23, 2020

Just Accepted

"Just Accepted" manuscripts have been peer-reviewed and accepted for publication. They are posted online prior to technical editing, formatting for publication and author proofing. The American Chemical Society provides "Just Accepted" as a service to the research community to expedite the dissemination of scientific material as soon as possible after acceptance. "Just Accepted" manuscripts appear in full in PDF format accompanied by an HTML abstract. "Just Accepted" manuscripts have been fully peer reviewed, but should not be considered the official version of record. They are citable by the Digital Object Identifier (DOI®). "Just Accepted" is an optional service offered to authors. Therefore, the "Just Accepted" Web site may not include all articles that will be published in the journal. After a manuscript is technically edited and formatted, it will be removed from the "Just Accepted" Web site and published as an ASAP article. Note that technical editing may introduce minor changes to the manuscript text and/or graphics which could affect content, and all legal disclaimers and ethical guidelines that apply to the journal pertain. ACS cannot be held responsible for errors or consequences arising from the use of information contained in these "Just Accepted" manuscripts.

is published by the American Chemical Society. 1155 Sixteenth Street N.W., Washington, DC 20036

Published by American Chemical Society. Copyright © American Chemical Society. However, no copyright claim is made to original U.S. Government works, or works produced by employees of any Commonwealth realm Crown government in the course of their duties.

3-Nitrene-2-Formylthiophene and 3-Nitrene-2-Formylfuran: Matrix-Isolation, Conformation, and Rearrangement Reactions

Jie Liu,[†] Zhuang Wu,[†] Yang Yang,[†] Weiyu Qian,[†] Lina Wang,[§] and Xiaoqing Zeng[†,§]*

[†]College of Chemistry, Chemical Engineering and Materials Science, Soochow University, 215123 Suzhou, China. E-mail: xqzeng@suda.edu.cn

[§]Department of Chemistry, Fudan University, Shanghai 200433, China. E-mail: xqzeng@fudan.edu.cn

ABSTRACT: Two new heteroarylnitrenes, 3-nitrene-2-formylthiophene (**15**/**15'**) and 3-nitrene-2-formylfuran (**16**/**16'**), in the triplet ground state have been generated in solid Ar (10.0 K) and N_2 (15.0 K) matrices by the 266 nm laser photolysis of 3-azido-2-formylthiophene (**13**) and 3-azido-2-formylfuran (**14**), respectively. According to the characterization with matrix-isolation IR spectroscopy and quantum chemical calculations at the B3LYP/6-311++G(3df,3pd) level, both nitrenes exhibit two conformations depending on the orientation of the formyl groups. Upon subsequent green-light irradiation (532 nm), both nitrenes **15**/**15'** and **16**/**16'** undergo ring-closure to form 3,2-thienoisoxazole (**17**) and 3,2-furoisoxazole (**18**), respectively. Traces of 3-imino-4,5-dihydrothiophene-2-ketene (**19**), formally formed through intramolecular 1,4-H shift in the corresponding nitrenes **15**/**15'**, have been also identified among the laser photolysis products of the azide **13**. In sharp contrast to the photochemistry, the high-vacuum flash pyrolysis (HVFP) of the azide **13** at ca. 1000 K mainly yields imino ketene in two conformations **19**/**19'** together with traces of isoxazole **17**. In addition to the reversible conformational interconversion in the imino ketene **19** ↔ **19'**, the photoisomerization from isoxazole **17** to imino ketene **19** has also been observed. The HVFP of the azide **14** at ca. 1000 K results in complete dissociation to HCN, C_2H_2, CO, CO_2, H_2O, and N_2. Unlike the recently disclosed hydrogen-atom tunneling (HAT) in the transformation from the structurally related 2-formyl phenylnitrene (**2**) to imino ketene **3** in cryogenic Ar-matrix, the absence of HAT in nitrenes **15** and **16** can be reasonably explained by the higher barrier heights and also larger barrier widths in the isomerization reactions.

INTRODUCTION

Arylnitrenes (Ar–N) are transient species that have been broadly used as highly reactive intermediates in synthetic nitrogenation reactions,[1] catalytic C–H amination and aziridination of olefins,[2] fabrication of crystalline molecular flasks,[3,4] and photolabeling in biology.[5] Generally, arylnitrenes can be facilely generated by the decomposition of the corresponding azide precursors through thermally or photolytically initiated N_2-elimination. However, rapid inter- and/or intramolecular reactions occurring under the formation conditions render the studies on the fundamental properties of this class of electron-deficient species challenging. As one of the most frequently studied arylnitrenes, the prototypical phenylnitrene was first proposed by Huisgen and co-workers in the decomposition of phenyl azide in the 1950s.[6–8] The first-time spectroscopic characterization of this triplet species was achieved when following the photolysis of the azide in cryogenic glassy matrix by using EPR spectroscopy in 1962.[9] Later on, the spectroscopy, structure, and reactivity of pheylnitrene[10] and diverse substituted derivatives[11–13] have been the topics of extensive experimental and computational studies in the past few decades. For instances, triplet phenylnitrene is a thermally persistent species in the gas phase that can be produced by pyrolysis of the corresponding azide.[14] However, 2-formyl phenylnitrene (**2**), which can be generated by photodecomposition of either 2-formyl phenylazide (**1**) or 2,1-benzisoxazole (**4**), isomerizes to 6-imino-2,4-cyclohexadien-1-ketene (**3**) through intramolecular 1,4-H shift (Scheme 1) even at 10.0 K via quantum mechanical tunneling (QMT).[15] This triplet species **2** can also undergo photo-induced isomerization to a benzazirine **5**, and the latter spontaneously coverts to a cyclic ketenimine by meanings of heavy-atom tunneling.[16] More recently, competitive nitrogen and carbon tunneling transformations have been observed during the transformation from an amino-substituted benzazirine to *p*-aminophenylnitrene and ketenimine in solid argon (3–18 K).[17]

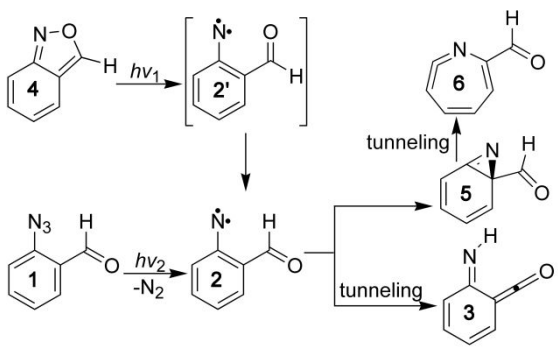

Scheme 1. The generation and isomerization of 2-formyl phenylnitrene (**2**).[15,16]

Similar to the rich chemistry of arylnitrenes, the fundamental properties of various heteroarylnitrenes[18] such as quinazolylnitrenes,[19] pyridylnitrenes,[20] and pyrrylnitrenes,[21] have also been intensively explored through the interplay of theory and experiment. In addition to the typical ring-expansion of arylnitrenes to cyclic ketenimines (e.g., **2** → **6** in Scheme 1),[16] most heteroarylnitrenes can undergo ring-opening reactions to yield nitriles.[22] For instances, triplet 2-pyridylnitrene prefers ring-expansion to cyclic carbodiimide as followed by further isomerization to phenylcarbene via ring-contraction.[23,24] Whereas, triplet 3-furylnitrene (**8**)[25] and 3-thienylnitrene (**11**),[26] generated in the photodecomposition of 3-furyl isocyanate (**7**) and 3-thienylsulfonyl nitrene (**10**) in cryogenic matrices, favors ring-opening to form nitriles **9** and **12** upon irradiation, no ring-expansion products could be identified.

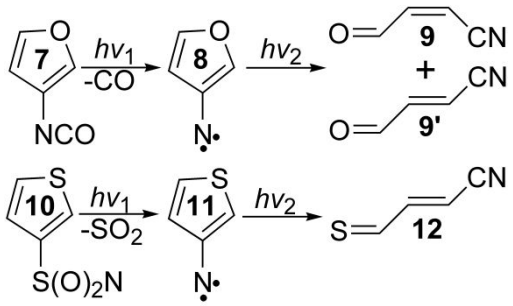

Scheme 2. The generation and isomerization of 3-furylnitrene (**8**)[25] and 3-thienylnitrene (**11**).[26]

The distinct reactivity associated with different aryl- and heteroarylnitrenes stimulates us to extend our study to 3-nitrene-2-formylthiophene (**15**) and 3-nitrene-2-formylfuran (**16**). Due to their structural similarity with 2-formyl phenylnitrene (**2**) (Scheme 1), 3-furylnitrene (**8**), and 3-thienylnitrene (**11**) (Scheme 2), intramolecular rearrangement processes such as ring-expansion, 1,4-H shift through quantum mechanical tunneling, and ring-opening reactions might be expected. Herein, we report a first-time study on the photochemistry of 3-azido-2-formylthiophene (**13**) and 3-azido-2-formylfuran (**14**) in solid Ar (10.0 K) and N_2 (15.0 K) matrices by combining matrix-isolation IR spectroscopy and quantum chemical calculations (Scheme 3). In addition to the identification of the two novel heteroarylnitrenes **15**/**15'** and **16**/**16'** in *syn*/*anti* conformations, the photo-induced ring-closure of nitrenes **15** and **16** to elusive isoxazoles **17** and **18** and the 1,4-H

shift of nitrene **15** to imino ketene **19** bypassing hydrogen-atom tunneling have been observed.

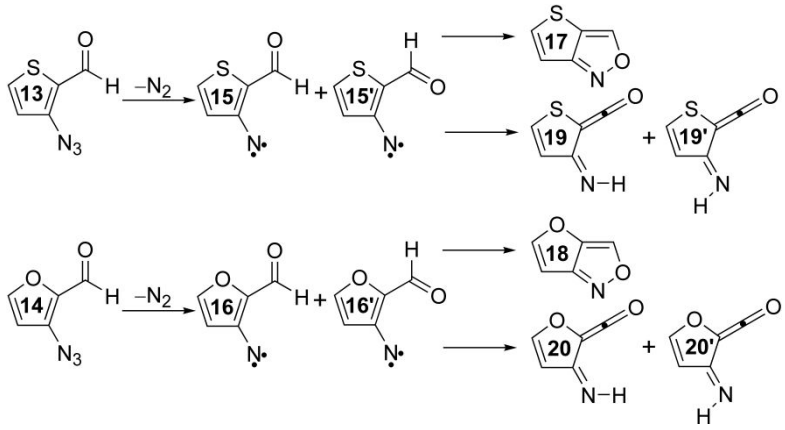

Scheme 3. Proposed photochemistry of 3-azido-2-formylthiophene (**13**) and 3-azido-2-formylfuran (**14**).

EXPERIMENTAL SECTION

Sample Preparation. 3-Azido-2-formylthiophene (**13**) was synthesized and purified according to the literature.[27] Briefly, a suspension of 3-bromo-2-formylthiophene (0.191 g, 1 mmol) and sodium azide (0.195 g, 3 mmol) in dimethyl sulfoxide (1.5 mL) was stirred at 65 ºC for 24 h. Then, the mixture was poured into water and extracted with ether. The combined extracts were evaporated, and the vapor of the yellow crude product was passed through two successive cold U-traps (–20 and –196 ºC). Pure azide **13** was retained in the first trap as solid. The quality of the sample was checked by NMR spectroscopy (Figure S1). ^{1}H NMR (600 MHz, DMSO-d6): δ = 9.82 (s), 8.15 (d, J = 5.4 Hz), 7.34 (d, J = 5.4 Hz) ppm and ^{13}C NMR (150 MHz, DMSO-d6): δ = 180.73, 145.68, 137.16, 127.15, 122.86 ppm.

3-Azido-2-formylfuran (**14**) was synthesized and purified in a similar manner. 3-Bromo-2-formylfuran (0.175 g, 1 mmol), sodium azide (0.195 g, 3 mmol), and dimethyl sulfoxide (1.5 mL) were used for the reaction. The solvent was poured into water and extracted with ether, and the organic layers were evaporated under reduced pressure. Then, the vapor of the residue was passed through two successive cold U-traps (–20 and –196 ºC), and pure azide **14** was retained in the first trap. The quality of the sample was checked by NMR spectroscopy (Figure S2). ^{1}H NMR (600 MHz, $CDCl_3$): δ = 9.71 (s), 7.62 (d, J = 1.8 Hz), 6.65 (d, J = 1.8 Hz) ppm and ^{13}C NMR (150 MHz, $CDCl_3$): δ = 176.42, 147.88, 116.85, 112.66, 106.70 ppm.

Matrix-isolation IR Spectroscopy. Matrix IR spectra were recorded on a FT-IR spectrometer

(Bruker 70V) in a reflectance mode using a transfer optic. A KBr beam splitter and liquid-nitrogen cooled MCT detector were used in the mid-IR region (4000–600 cm^{-1}). For each spectrum, 200 scans at a resolution of 0.5 cm^{-1} were coadded.

The solid sample was mixed by passing a flow of Ar or N_2 gas through a U-trap containing ca. 20 mg of the azide (**13**: 19 °C and **14**: 33 °C). Then the mixture (azide/dilution gas ≈ 1 : 1000 estimated) was passed through an aluminum oxide furnace (o.d. 2.0 mm, i.d. 1.0 mm), which can be heated over a length of ca. 25 mm by a tantalum wire (o.d. 0.4 mm, resistance 0.4 Ω) and immediately deposited (2 mmol h^{-1}) at a high vacuum onto the Rh-plated copper block matrix support (Ar: 10.0 K; N_2: 15.0 K) in high vacuum (~10^{-6} Pa), using a closed-cycle helium cryostat (Sumitomo Heavy Industries, SRDK-408D2-F50H) inside the vacuum chamber. The electric power (voltage/current) used in pyrolysis experiments was 5.4 V/3.6 A. Photolysis experiments were performed by using a Nd^{3+}:YAG laser (266 nm, 532 nm, MPL-F-266, 10 mW), and a high-power flashlight (Boyu T648, 365 nm, 20 W).

Computational Details. Structural optimizations were performed using density functional theory (DFT) methods of B3LYP,[28] mPW1PW9[29] and M06-2X[30] combined with the 6-311++G(3df,3pd) basis set. Accurate relative energies of the species were further calculated by using the complete basis set CBS-QB3[31] and CCSD(T)[32] methods. For the CCSD(T) single-point calculations, the 6-311++G(3df,3pd) basis set and the B3LYP/6-311++G(3df,3pd) optimized structures were used. In addition, the energies of the nitrenes in the closed-shell singlet (CCS) state, open-shell singlet (OSS) state, and triplet state were also calculated by applying the second-order multiconfigurational perturbation theory (CASPT2) method (referred to as "RS2C" in Molpro),[33] which accounts for dynamic correlation, using the complete active space SCF (CASSCF) wave functions as references in the RS2C calculation. The active space includes 8 electrons and 8 active orbitals, namely, CASPT2(8,8). All the CASPT2 calculations were carried out with the CASSCF(8,8)/cc-pVTZ optimized geometries. Time-dependent (TD)[34,35] calculations were performed at the B3LYP/6-311++G(3df,3pd) level for the prediction of UV/Vis transitions. Local minima were confirmed by vibrational frequency analyses, and transition states by additional intrinsic reaction coordinate (IRC) calculations.[36,37] For tunneling computations on the triplet manifold we used the calculated potential energy data along the intrinsic reaction path at the B3LYP/6-311++G(3df,3pd) level. The intrinsic reaction coordinate (IRC) was computed in

nonmass-weighted Cartesian coordinates, by using the "IRC=Cartesian" option, expressed in units of Bohr. The DFT and CBS-QB3 calculations were performed using the Gaussian 09 software package.[38] The CCSD(T), CASPT2, and CASSCF calculations were performed with the MOLPRO 2012 program.[39]

RESULTS AND DISCUSSION

Photochemistry of 3-azido-2-formylthiophene (13)

The photolysis of 3-azido-2-formylthiophene (**13**) in solid Ar-matrix at 10.0 K was performed by using a 266 nm laser. After 11 s of irradiation, half of the azide decomposes and yields new species with strong IR bands at 2140.4, 2129.1, 1663.9, 1649.4, 1243.4, 1186.1, 740.6, and 678.2 cm^{-1}. The first two bands are close to the frequencies for the characteristic asymmetric CCO stretching vibration modes ν_{asym}(C=C=O) found in ketenes such as **3** (2149 cm^{-1}, Ar-matrix).[15] Therefore, it is very likely that the 1,4-H shift product imino ketene **19** of the nitrene intermediate **15** (Scheme 3) forms during the laser photolysis of the azide **13**. The formation of imino ketene **19** is also supported by the observation of two weak but distinguishable IR bands at 3310.2 and 3292.5 cm^{-1} for the N–H stretching vibrations in the two conformers (vide infra).

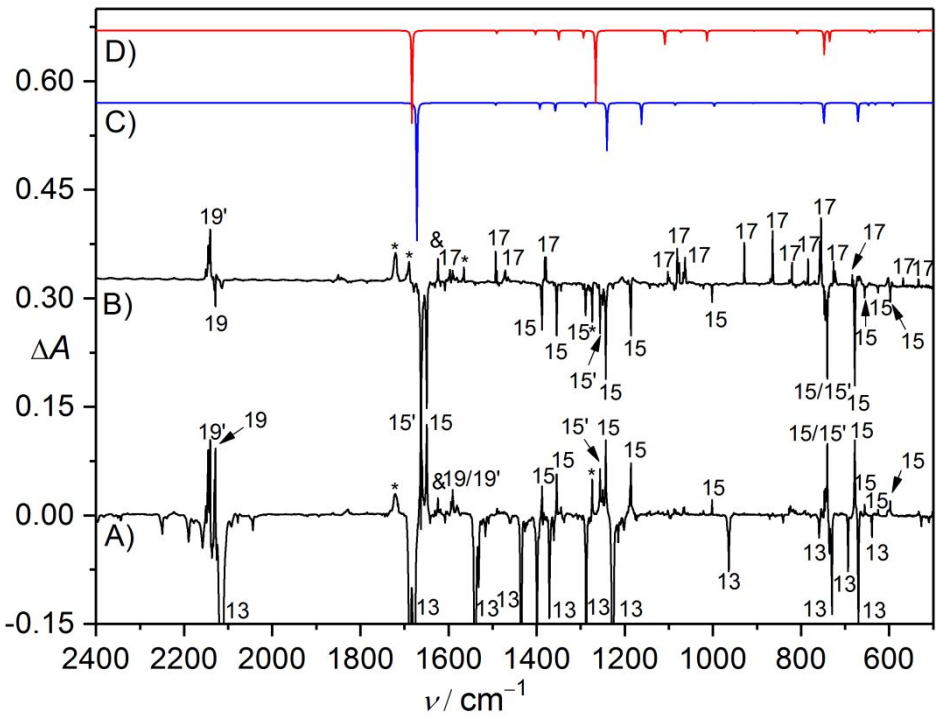

Figure 1. (A) IR difference spectrum showing the decomposition of 3-azido-2-formylthiophene (**13**) in Ar-matrix (10.0 K) upon 266 nm laser irradiation (11 s). (B) IR difference spectrum showing the rearrangement of nitrenes

15 (*syn*) and **15'** (*anti*) to isoxazole **17** upon subsequent visible light irradiation (532 nm, 15 min). (C, D) B3LYP/6-311++G(3df,3pd) calculated IR spectra (scaled by a factor of 0.98) for nitrenes **15** (*syn*) and **15'** (*anti*) in the triplet state. Bands of imino ketenes **19** (*syn*), **19'** (*anti*), H_2O (&), and unknown species (*) are also marked.

Considering the TD-B3LYP/6-311++G(3df,3pd) calculated absorptions at 493 nm (**15**: oscillator strength f = 0.0106) and 480 nm (**15'**: f = 0.0104) for the nitrene intermediate **15** in the triplet ground state (Table S1), the matrix containing the 266 nm laser photolysis of the azide **13** was further irradiated with green light (532 nm). As a result, all the IR bands associated with the nitrenes **15** and **15'** vanish completely and another set of IR bands (**17**) forms concomitantly (Figure 1B). Simultaneously, conversion occurs to the two conformers of imino ketene **19** (*syn* → *anti*) under the irradiation conditions. Among the depleted IR bands (Figure 1B, bands pointing downward), the two strongest ones at 1663.9 and 1649.4 cm^{-1} can be reasonably assigned to the C=O stretching vibrational modes ν(C=O) in the two conformers of the expected nitrene **15**, which differ mainly in the orientation of the two C=O groups (Scheme 3). The frequencies are slightly red-shifted in comparison with the ν(C=O) mode in the azide precursor **13** (1689.1/1678.6 cm^{-1} in Ar-matrix). This assignment is also supported by the good agreement of the observed band positions (1663.9 and 1649.4 cm^{-1}) with the B3LYP/6-311++G(3df,3pd) calculations at 1683 and 1672 cm^{-1} for the *anti* and *syn* conformers of nitrene **15** in the triplet state (Table 1). In contrast, the calculated ν(C=O) modes in the two conformers of the nitrene **15** in the higher-energy closed-shell singlet state locate at 1713 (*syn*) and 1748 cm^{-1} (*anti*, Table S2). Interestingly, there are two weak IR bands at 1720.7 and 1689.3 cm^{-1} (bands marked with asterisks in Figure 1B) appear after the depletion of the triplet nitrene, their intensities keep increasing even after further 266 nm laser irradiation. According to the TD-B3LYP/6-311++G(3df,3pd) calculations (Table S1), the two conformers of the singlet nitrene **15** display intense absorptions at 270 (*syn*) and 278 nm (*anti*), the unexpected photobehavior renders the assignment of these two bands to the nitrene in the singlet state unlikely. It should be noted that magnetically bistable nitrenes[25,40] and closely related carbene analogues[41] have been recently observed in cryogenic matrices.

Table 1. Calculated and experimentally observed IR frequencies of nitrenes **15** (*syn*) and **15'** (*anti*).

calculated[a]				observed[b]				sym	approximate
CSS		triplet		Ar-matrix		N_2-matrix			assignment[c]
syn	*anti*	*syn*	*anti*	*syn*	*anti*	*syn*	*anti*		
3182 (<1)	3184 (<1)	3179 (<1)	3181 (<1)					A'	ν(CH)
3159 (1)	3160 (1)	3161 (1)	3161 (1)					A'	ν(CH)
2964 (11)	2829 (77)	2895 (39)	2847 (78)	2858.9 w		2860.2 vw		A'	ν(OC–H)
1713 (190)	1748 (166)	1672 (275)	1683 (198)	1649.4 s	1663.9 s	1651.1 s	1662.6 m	A'	ν(C=O)
1494 (8)	1487 (15)	1493 (4)	1491 (6)					A'	ν(C=C)
1417 (90)	1422 (18)	1393 (13)	1402 (8)	1389.7		1391.8 m		A'	ρ(OC–H)
1349 (9)	1391 (61)	1358 (19)	1349 (22)	1354.8	1345.1 w	1355.0 m	1348.7 vw	A'	ν(CN) + ρ(CH)
1282 (33)	1275 (12)	1290 (9)	1294 (15)	1289.2	1293.8 w	1291.2 m	1295.7 vw	A'	ρ(CH)
1243 (65)	1230 (106)	1241 (97)	1266 (144)	1243.4 s	1256.4 m	1249.2 m	1260.7 m	A'	ν(C=C)
1137 (21)	1096 (3)	1162 (45)	1109 (29)	1186.1	1143.6 vw	1190.3 m	1132.5 w	A'	ν(C–C_{ring})
1064 (15)	1031 (36)	1086 (4)	1073 (4)	1088.0 w		1090.4 w		A'	ρ(CH)
1025 (<1)	1007 (29)	997 (7)	1013 (22)	1002.4 w	1022.3 vw	1005.1 w	1024.1 vw	A'	ρ(CH)
969 (22)	991 (<1)	982 (<1)	975 (<1)					A"	ω(OC–H)
940 (<1)	942 (1)	907 (<1)	907 (<1)					A"	τ(CH)
771 (2)	786 (3)	800 (2)	809 (7)					A'	ν(CS)
761 (42)	759 (43)	748 (49)	748 (49)	740.6 s	740.6 s	751.6 m	751.6 m	A"	ω(CH)
685 (72)	677 (56)	670 (44)	735 (22)	678.2 s	737.2 w	681.2 s	745.3 w	A'	ν(CS)
653 (7)	649 (4)	648 (5)	644 (5)	655.9 w		656.0 w		A'	ring distortion
642 (8)	646 (7)	631 (4)	634 (4)	625.4 vw		626.0 vw		A"	ring distortion
591 (10)	543 (5)	592 (6)	533 (3)					A'	ring breathing
495 (<1)	472 (<1)	465 (4)	438 (1)					A'	ring distortion
486 (<1)	406 (15)	442 (2)	411 (9)					A"	ring distortion
337 (2)	398 (2)	319 (<1)	375 (7)					A'	ρ(CN)
276 (8)	242 (<1)	287 (3)	262 (<1)					A"	ring distortion
244 (12)	186 (16)	189 (14)	206 (11)					A"	ω(CN) + ω(OC–H)
170 (12)	184 (<1)	158 (9)	160 (3)					A'	ρ(OC–C)
101 (4)	−69 (<1)	123 (<1)	111 (<1)					A"	ω(C=O)

[a]Calculated harmonic IR frequencies (cm^{-1}, scaled by a factor of 0.98)[42] and intensities ($km\ mol^{-1}$, in parentheses) for the closed-shell singlet (CSS) and triplet states at the B3LYP/6-311++G(3df,3pd) level. [b]Observed band positions of the most intense matrix sites in Ar- and N_2-matrices. The relative band intensities: s = strong, m = medium strong, w = weak, vw = very weak. [c]Tentative assignment based on the calculated vibrational displacement vectors for the *syn*-conformer in the triplet state.

In line with the calculated frequencies of 1358 and 1349 cm^{-1} for the C–N stretching vibrations in the two conformers of triplet nitrene **15**, two weak bands at 1354.8 and 1345.1 cm^{-1} can be clearly identified. And, they are quite close to the ν(C–N) modes in the parent triplet 3-thienylnitrene (**11**) (1350.2 cm^{-1}, Ar-matrix)[26] and phenylnitrene (1312.3 cm^{-1}, Ne-matrix).[43,44] The generation of nitrene **15** in the 266 nm laser photolysis of azide **13** is reproducible when using N_2 as the matrix host (Figure S3). The observed band positions of triplet nitrene **15** in N_2-matrix shift slightly (< 12 cm^{-1}, Table 1) due to different weak interactions with the surrounding matrix materials. Attempts to stimulate the conformational conversion between the two conformers of

nitrene **15** failed by annealing the matrix to 25.0 K or irradiating with visible-light (830 and 532 nm), and mainly the transformation from nitrene **15** to isoxazole **17** happens under the irradiation conditions.

Unlike the spontaneous tunneling transformation from triplet 2-formyl phenylnitrene (**2**) to singlet imino ketene **3** in Ar-matrix at 10.0 K (Scheme 1),[15] the two conformers of nitrene **15** are stable in both Ar- and N_2-matrices, no noticeable change of their IR bands could be observed when keeping the corresponding matrix in the dark up to 25.0 K. In fact, the photo-induced conversion from nitrene **15** to imino ketenes **19**/**19'** via 1,4-H shift is much less efficient when comparing with the intramolecular cyclization to 3,2-thienoisoxazole (**17**, bands pointing upward in Figure 1B). In sharp contrast, no analogous cyclization of nitrene **2** to form an isoxazole **4** was observed, which is probably due to the sole formation of the unfavourable *anti*-conformer nitrene **2** in the photolysis of the azide precursor **1**, since the carbonyl oxygen atom in this configuration points away from the electron-deficient nitrene center. Unexpectedly, the previous attempt to generate the *syn*-conformer nitrene **2'**, in which the carbonyl oxygen atom points towards the electron-deficient nitrene center, through photo-induced ring-opening of the isoxazole **4** (Scheme 1) only yields the *anti*-conformer nitrene **2**.[15]

As can be seen in Figure 1A, only traces of imino ketene **19** are produced in the photolysis of the azide **13**. In fact, the calculated moderate activation barrier (< 20 kcal mol^{-1}) for the nitrene **2** → imino ketene **3** transformation[15] suggest that it may occur easily once the nitrene could be generated in the gas phase. As expected, the high-vacuum flash pyrolysis (HVFP) of the azide **13** at ca. 1000 K mainly yields imino ketene **19** together with traces of the cyclization isomer isoxazole **17** (Figure 2A). Similar to the photo-induced *syn* ↔ *anti* isomerization in other imines in matrices,[45] subsequent irradiation of the matrix containing the Ar-matrix isolated HVFP products with UV-light (365 nm) results in selective *anti* → *syn* conversion in imino ketene **19** (Figure 2B), whereas, further 266 nm laser irradiation leads to the reverse conversion (Figure 2C). It is noteworthy that the transformation from isoxazole **17** to imino ketene **19** also occurs under the laser irradiation conditions, which is probably due to the formation of nitrene (isoxazole **17** → nitrene **15**) as followed by concomitant 1,4-H migration (nitrene **15** → imino ketene **19**). The dominant formation of imino ketene **19** in the thermal decomposition of 3-azido-2-formylthiophene (**13**) is in sharp contrast to the pyrolysis of the closely related

2-acetyl-3-azidothiophene, in which the major product is 3-methylthieno[3,2-*c*]isoxazole.[46]

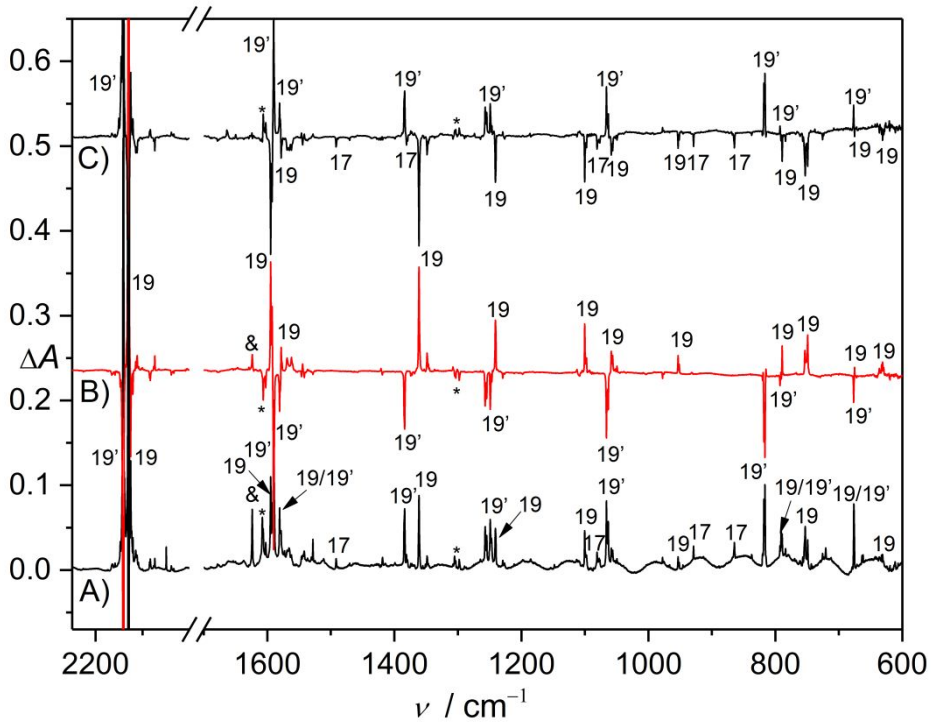

Figure 2. (A) Ar-matrix IR spectrum of the high-vacuum flash pyroysis (ca. 1000 K) products of 3-azido-2-formylthiophene (**13**). (B) IR difference spectrum showing rearrangement of imino ketenes **19'** (*anti*) to **19** (*syn*) upon UV-light irradiation (365 nm, 25 min). (C) IR difference spectrum showing rearrangement of imino ketenes **19** (*syn*) to **19'** (*anti*) upon 266 nm laser irradiation (2 min). Bands of isoxazole **17**, H_2O (&), and unknown species (*) are also marked.

The reversible photo-interconversion between the two conformers of imino ketene **19** allows unambiguously identification of all the IR bands in the range of 4000–600 cm^{-1} (Table 2 and Table S3). The observed difference of 11.3 cm^{-1} between the two ν_{asym}(C=C=O) modes in the *anti* and *syn* conformers agrees with the calculation (12 cm^{-1}) at the B3LYP/6-311++G(3df,3pd) level. The weaker C=N stretching modes for the two conformers locate at 1590.1 and 1594.7 cm^{-1}, coinciding with the calculated frequencies of 1601 and 1603 cm^{-1}, respectively. According to the calculated and observed IR intensities for the two well-resolved bands at 1384.1 (*anti*) and 1361.2 cm^{-1} (*syn*), a ratio of 1: 0.8 for the two conformers among the HVFP products of the azide **13** can be estimated. This is in consistent with the calculated lower energy of the *anti*-conformer than the

syn-conformer by 1.0 kcal mol^{-1}. The assignment of the bands (1596.8, 1493.1, 1471.1, 1381.8, 1102.3, 1081.2, 1063.4, 928.9, 865.1, 821.0, 784.7, 754.8, 726.4, and 683.8 cm^{-1}) to the cyclization product isoxazole **17** (Figure 1B) is also supported by the agreement with the calculated IR fundamental modes (Table S4).

Table 2. Calculated and experimentally observed IR frequencies for the *syn* and *anti* conformers of imino ketene **19**.

calculated[a]		observed[b]			approximate
syn	*anti*	*syn*	*anti*	sym	assignment[c]
3413 (9)	3422 (7)	3292.5 vw	3310.2 vw	A'	ν(NH)
3171 (<1)	3165 (<1)			A'	ν(CH)
3154 (2)	3140 (<1)			A'	ν(CH)
2162 (1049)	2174 (1062)	2129.1 s	2140.4 s	A'	ν_{asym}(C=C=O)
1603 (232)	1601 (275)	1594.7 m	1590.1 m	A'	ν(C=N)
1556 (36)	1544 (17)	1578.1 w	1580.8 w	A'	ν(C=C$_{ring}$)
1352 (104)	1378 (52)	1361.2 m	1384.1 w	A'	ν_{sym}(C=C=O)
1305 (5)	1301 (8)	1307.8 vw	1303.5 vw	A'	ρ(CH)
1240 (47)	1249 (101)	1241.1 w	1249.2 w	A'	ρ(CH) + ρ(NH)
1100 (40)	1100 (4)	1100.4 w		A'	δ(CH) + ρ(NH)
1038 (35)	1045 (58)	1058.5 w	1066.2 w	A'	ρ(CH) + ρ(NH)
933 (14)	967 (1)	953.4 vw		A'	δ_{ip}(C=C=O)
916 (<1)	907 (1)			A"	τ(CH)
813 (11)	819 (98)	814.6 vw	816.6 m	A"	τ(NH)
782 (23)	784 (11)	789.3 w	792.8 vw	A'	ring breathing
758 (82)	732 (<1)	753.0 w		A"	ω(CH) + ω(NH)
670 (22)	672 (31)	675.3 vw	676.6 vw	A'	ring breathing
638 (21)	646 (7)	631.0 vw		A"	ω(CH)
626 (9)	621 (<1)			A'	ring breathing
554 (2)	552 (5)			A'	ν(CS)
519 (7)	524 (18)			A"	δ_{oop}(C=C=O)
458 (1)	463 (11)			A'	ring breathing
384 (3)	388 (<1)			A"	ring distortion
375 (10)	366 (2)			A'	ρ(CH)
215 (<1)	209 (<1)			A"	ring distortion
123 (2)	130 (<1)			A'	ρ(C=C=O)
72 (<1)	81 (4)			A"	ω(C=C=O)

[a]Calculated harmonic IR frequencies (cm^{-1}, scaled by a factor of 0.98)[42] and intensities (km mol^{-1}, in parentheses) at the B3LYP/6-311++G(3df,3pd) level. [b]Observed band positions of the most intense matrix sites in Ar-matrix. The relative band intensities: s = strong, m = medium strong, w = weak, vw = very weak. [c]Tentative assignment based on the calculated vibrational displacement vectors for the *syn*-conformer.

Photochemistry of 3-azido-2-formylfuran (14)

Similar to the photochemistry of 3-azido-2-formylthiophene (**13**), the 266 nm laser photolysis of 3-azido-2-formylfuran (**14**) in solid N_2-matrix at 15.0 K causes N_2-elimination and furnishes 3-nitrene-2-formylfuran (**16** and **16'**) in *syn* and *anti* conformations (Figure 3A). Additionally, the presence of the 1,4-H migration product imino ketene **20** in *syn* and *anti* conformations can also be inferred by the appearance of two weak IR bands at 2137.0 and 2145.5 cm^{-1} for the characteristic ν_{asym}(C=C=O) modes in the spectrum. The two conformers of nitrene **16** are stable when keeping the matrix in the dark up to 25.0 K. Consistent with the calculated absorption at around 470 nm for the two conformers of the nitrene **16** (Table S1), subsequent visible-light irradiation (532 nm) promotes cyclization of the nitrene to form isoxazole **18** (Table S4). Additionally, the *syn* → *anti* conformational conversion in imino ketene **20** occurs simultaneously (Figure 3B).

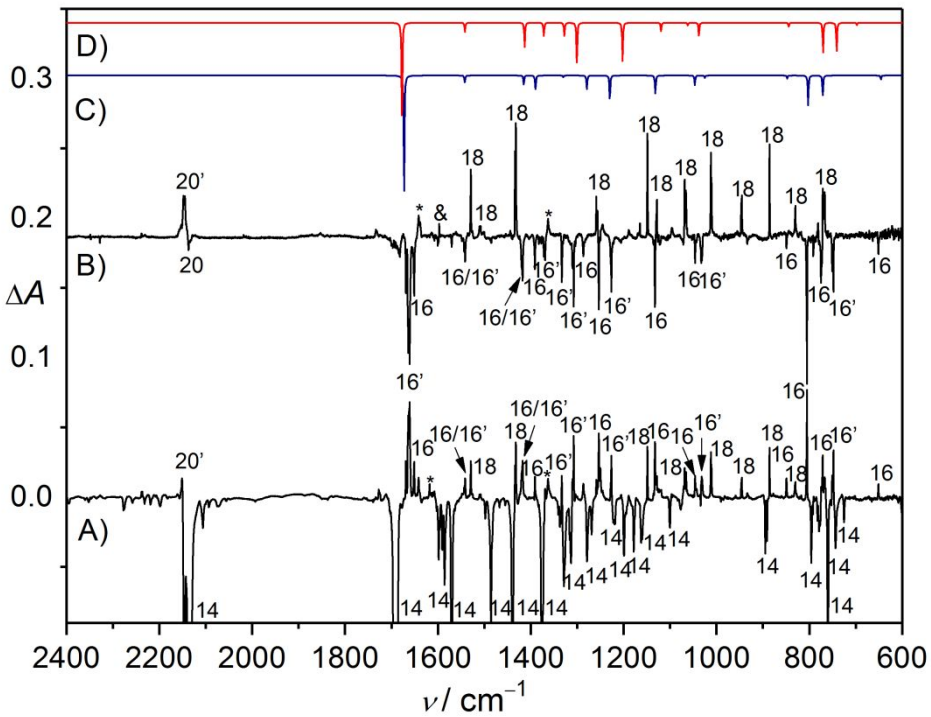

Figure 3. (A) IR difference spectrum showing the decomposition of 3-azido-2-formylfuran (**14**) in N_2-matrix (15.0 K) upon 266 nm laser irradiation (55 s). (B) IR difference spectrum (3 times expanded along the ΔA axis) showing the rearrangement of nitrenes **16** and **16'** to isoxazole **18** upon subsequent visible-light irradiation (532 nm, 55 min). (C, D) B3LYP/6-311++G(3df,3pd) calculated IR spectra (scaled by a factor of 0.98) for **16** (C: *syn*) and **16'** (D: *anti*) in the triplet state. Bands of imino ketenes **20**/**20'**, H_2O (&), and unknown species (*) are also marked.

The identification for the two conformers of nitrene **16** in the triplet ground state is supported

by the agreement with the calculated spectra (Table 3). Specifically, the characteristic ν(C=O) modes in the *syn* (**16**) and *anti* (**16'**) conformers appear at 1649.6 (cal. 1673 cm^{-1}) and 1662.2 cm^{-1} (cal. 1678 cm^{-1}, Table S5), respectively. They are quite similar to the ν(C=O) vibrational modes in triplet nitrene **15** (*syn*: 1649.4 cm^{-1}; *anti*: 1663.9 cm^{-1}). The ν(CN) mode in the *syn*-conformer of nitrene **16** could not be identified due to low IR intensity of 4 km mol^{-1}. In contrast, it appears at 1331.9 cm^{-1} in the *anti*-conformer (**16'**) with a calculated IR intensity of 25 km mol^{-1}. The photochemistry of the azide **14** in N_2-matrix is reproducible in Ar-matrix (Figure S4), in which the bands for nitrene **16** slightly shift by about 10 cm^{-1} (Table 3). In sharp contrast to the thermal decomposition of azide **13** (→ isoxazole **17** + imino ketene **19** + N_2), the pyrolysis of azide **14** at ca. 1000 K mainly leads to complete fragmentation products HCN, C_2H_2, CO, CO_2, H_2O, and N_2 (IR inactive) together with traces of the 1,4-H shift product imino ketene **20** (Figure S5).

Table 3. Calculated and observed IR frequencies of *syn* and *anti* conformations of nitrene **16**.

calculated[a]				observed[b]				sym	approximate assignment[c]
CSS		triplet		Ar-matrix		N_2-matrix			
syn	*anti*	*syn*	*anti*	*syn*	*anti*	*syn*	*anti*		
3224 (<1)	3221 (1)	3217 (<1)	3217 (<1)					A'	ν(CH)
3198 (3)	3201 (2)	3199 (3)	3198 (3)					A'	ν(CH)
2965 (10)	2864 (55)	2895 (38)	2877 (75)	2864.1 vw		2860.3 vw		A'	ν(OC–H)
1735 (169)	1676 (208)	1673 (265)	1678 (171)	1649.6 m	1662.2 s	1651.1 m	1660.9 s	A'	ν(C=O)
1549 (15)	1591 (8)	1542 (19)	1542 (16)	1540.2 m	1540.2 m	1541.5 m	1541.5 m	A'	ν(C=C)
1478 (29)	1551 (4)	1415 (21)	1413 (40)	1417.1 m	1417.1 m	1417.6 m	1417.6 m	A'	ρ(OC–H)
1392 (110)	1391 (42)	1390 (35)	1372 (23)	1387.9 m	1367.1 m	1391.1 m	1369.3 m	A'	ρ(CH)
1379 (55)	1315 (4)	1330 (4)	1328 (25)		1331.9 m		1333.3 m	A'	ν(CN) + ρ(CH)
1287 (21)	1242 (172)	1280 (34)	1300 (74)	1282.7 w	1306.3 m	1286.9 w	1307.6 m	A'	ν(C–C_{ring}) + ρ(CH)
1237 (108)	1168 (135)	1230 (57)	1202 (67)	1249.7 m	1223.5 m	1250.3 m	1226.7 m	A'	ν(C=C)
1096 (18)	1108 (4)	1132 (44)	1119 (14)	1133.9 m	1120.8 w	1132.6 m	1121.2 vw	A'	ρ(CH)
1078 (2)	1011 (7)	1047 (22)	1062 (5)	1042.2 m	1073.1 vw	1046.0 w	1072.0 vw	A'	ν(CO_{ring}) + ρ(CH)
997 (10)	951 (15)	1025 (6)	1038 (21)		1035.0 m		1033.0 w	A'	ν(C–C_{ring}) + ρ(CH)
914 (19)	925 (4)	971 (<1)	969 (<1)					A"	ω(OC–H)
910 (<1)	880 (4)	882 (<1)	879 (<1)					A"	τ(CH)
831 (3)	823 (5)	848 (7)	845 (7)	848.8 w	848.8 w	849.4 vw	849.4 vw	A'	ring breathing
790 (51)	771 (57)	803 (69)	770 (50)	805.3 s	766.7 m	805.5 s	774.8 m	A'	ring breathing
782 (31)	719 (49)	771 (48)	741 (50)	766.7 m	748.4 m	774.8 m	748.3 m	A"	ω(CH)
716 (21)	688 (49)	654 (<1)	698 (4)					A"	ring distorting
694 (3)	643 (4)	646 (9)	658 (<1)	649.3 vw		651.3 vw		A'	ring breathing
655 (20)	525 (5)	569 (6)	559 (8)					A"	ring distorting
539 (4)	468 (4)	529 (4)	470 (2)					A'	ring distorting

340 (2)	416 (10)	328 (<1)	388 (19)	A'	ρ(CN)
299 (4)	266 (8)	314 (3)	276 (<1)	A"	ω(CN) + ω(OC–H)
268 (11)	191 (9)	217 (16)	233 (13)	A"	ω(CN) + ω(OC–H)
178 (14)	135 (3)	175 (10)	162 (1)	A'	ρ(OC–C)
106 (8)	100 (2)	129 (1)	128 (<1)	A"	ω(C=O)

[a]Calculated harmonic IR frequencies (cm^{-1}, scaled by a factor of 0.98)[42] and intensities (km mol^{-1}, in parentheses) for the closed-shell singlet (CSS) and triplet states at the B3LYP/6-311++G(3df,3pd) level. [b]Observed band positions of the most intense matrix sites in Ar- and N_2-matrices. The relative band intensities: s = strong, m = medium strong, w = weak, vw = very weak. [c]Tentative assignment based on the calculated vibrational displacement vectors for the *syn*-conformer in the triplet state.

Quantum Chemical Calculations

To understand the mechanism for the observed rearrangement reactions of the two structurally related heteroarylnitrenes **15** and **16**, their potential energy profiles in the closed-shell singlet state (CSS) have been computationally explored at the CCSD(T)/aug-cc-pVTZ//B3LYP/6-311++G(3df,3pd) level, and the results for nitrene **16** are depicted in Figure 4 (Figure S6 for nitrene **15**).

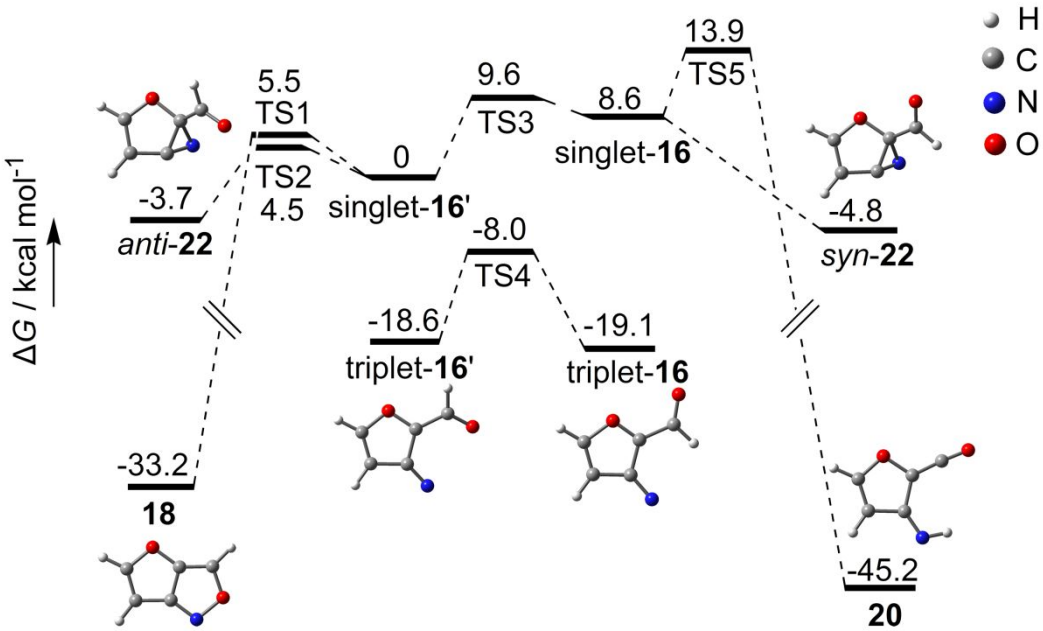

Figure 4. Calculated relative Gibbs free energy profile (kcal mol^{-1}, including zero-point vibrational energy corrections) for the rearrangement of closed-shell singlet state 3-nitrene-2-formylfuran (**16**) at the CCSD(T)/aug-cc-pVTZ//B3LYP/6-311++G(3df,3pd) level.

For 3-nitrene-2-formylfuran (**16**) in the CSS state, the *anti*-conformer (**16'**) is lower in energy than the *syn*-conformer (**16**) by 8.6 kcal mol^{-1}. In contrast, the *syn*-conformer becomes more stable

in the triplet ground state by 0.5 kcal mol^{-1}. The calculated activation barrier between the two conformers in the triplet state is more than 10 kcal mol^{-1}, rendering the thermally initiated conformational conversion in cryogenic matrices (< 25.0 K) unlikely. Furthermore, the large energy gaps (ΔE_{ST}) between the CSS and triplet states for nitrene **16** (*anti*: 18.6 kcal mol^{-1}; *syn*: 27.7 kcal mol^{-1}) suggest that the initially generated singlet nitrene may immediately relax to the triplet state through rapid intersystem crossing (ISC) at low temperatures. By analogy, the two conformers for 3-nitrene-2-formylthiophene (**15**) in the triplet ground state differ by 2.7 kcal mol^{-1}, and the barrier associated with the conformational conversion from the *anti*-conformer (**15'**) to lower-energy *syn*-conformer (**15**) is 6.9 kcal mol^{-1} (Figure S6). Similar to the electronic properties of phenylnitrene,[47] the calculations with the second-order multiconfigurational perturbation theory (CASPT2) on the two heteroarylnitrenes **15**/**15'** and **16**/**16'** demonstrate that the open-shell singlet (OSS) state is higher in energy than the triplet ground state by about 15 kcal mol^{-1} at the CASPT2(8,8)/cc-pVTZ//CASSCF(8,8)/cc-pVTZ level. Furthermore, the CSS state is above the OSS state by about 20 kcal mol^{-1} (Table 4).

Table 4. Calculated energy gaps ΔE_{ST} (kcal mol^{-1}) between the closed-shell singlet state and the triplet state for nitrenes **15** and **16**.

species	B3LYP[a]	CBS-QB3	CCSD(T)[b]	mPW1PW9[a]	CASPT2[c]
syn-**15**	29.7	28.8	26.6	33.5	33.6 (15.3)
anti-**15'**	35.5	34.9	32.6	39.4	36.0 (14.9)
syn-**16**	30.2	28.9	27.7	34.5	33.6 (15.7)
anti-**16'**	27.2	18.0	18.6	31.5	36.1 (15.2)

[a]At the 6-311++G(3df,3pd) basis set. [b]At the CCSD(T)/aug-cc-pVTZ//B3LYP/6-311++G(3df,3pd) level. Positive values refer to the triplet being more stable. [c]At the CASPT2(8,8)/cc-pVTZ//CASSCF(8,8)/cc-pVTZ level. The energy gaps between the open-shell singlet state and the triplet state are given in parentheses.

In addition to the ISC to the triplet ground state, CSS singlet nitrene *anti*-**16'** may undergo cyclization to form either isoxazole **18** or azirine **22** through the attack the electron-deficient nitrene center to the carbonyl oxygen or carbon atoms by overcoming comparable activation barriers of 5.5 (TS1) and 4.5 kcal mol^{-1} (TS2), respectively. The former pathway is thermodynamically more favorable due to large energy release of 33.2 kcal mol^{-1}. This is fully consistent with the experimental observation of the isomerization of nitrene **16** to isoxazole **18** in

matrix (Figure 3). The simultaneous formation of traces of imino ketene **20** from nitrene **16** can also be explained by even larger energy release of 45.2 kcal mol^{-1}, while the activation barrier is higher by 8.4 kcal mol^{-1}, which makes this pathway less competitive than forming isoxazole **18** (Figure 4). Alternatively, the formation of imino ketene **20** might be caused by the photo-induced 1,4-H migration in isoxazole **18** with concerted N–O bond fragmentation. In line with the observation of imino ketene **19** among the pyrolysis products of the azide precursor **13**, the 1,4-H shift in nitrene **15** to imino ketene **19** is more exothermic than the cyclization to 3,2-thieno isoxazole (**17**), and the latter has been obtained during the laser photolysis of the azide **13** under matrix-isolation conditions.

Recently, the spontaneous conversion of triplet 2-formyl phenylnitrene (^{3}**2**) to singlet 6-imino-2,4-cyclohexadien-1-ketene (^{1}**3**) has been observed in solid Ar-matrix at 10.0 K, for which a mechanism of hydrogen-atom tunneling (HAT) has been proposed.[15] The tunneling mechanism has analyzed by estimating the barrier height 17.2 kcal mol^{-1} (Figure S7) and the barrier width 2.50 Bohr for the 1,4-H migration from nitrene ^{3}**2** to imino ketene ^{3}**3** according to intrinsic reaction coordinate (IRC) scans at the B3LYP/6-311++G(3df,3pd) level (Figure 5). As a further step, the putative triplet imino ketene ^{3}**3** immediately relaxes to the singlet ground state ^{1}**3** in the cryogenic matrix.

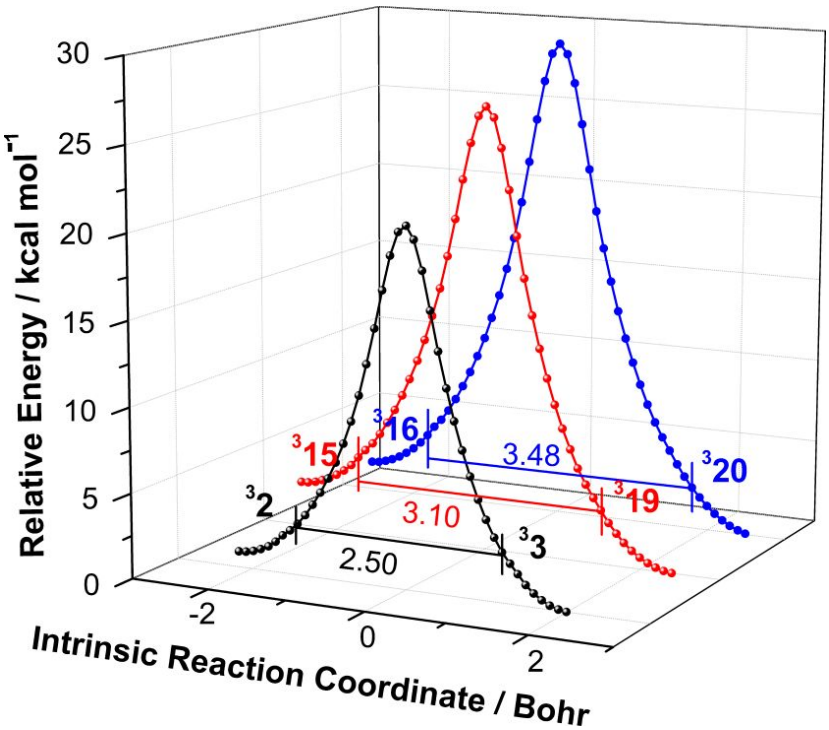

Figure 5. B3LYP/6-311++G(3df,3pd) calculated intrinsic reaction coordinate (IRC) profiles for rearrangement of

triplet nitrenes (^{3}**2**, *syn*-^{3}**15**, and *syn*-^{3}**16**) to triplet ketenes (^{3}**3**, *syn*-^{3}**19**, and *syn*-^{3}**20**) via intramolecular 1,4-H shift. The estimated widths of the barriers (in Bohr) are also indicated.

According to the Jeffreys-Wentzel-Kramers-Brillouin (JWKB) approximation (Eq 1),[48] the tunneling probability P(E) through a parabolic barrier depends on the mass (m) of the tunneling atom, the width of barrier (w), and the height of the barrier (V_0–E). The calculated tunneling probability P(E) for nitrene ^{3}**2** to form ketene ^{3}**3** was estimated to be 7.14 × 10^{-18} at the B3LYP/6-311++G(3df,3pd) level. Since the tunneling rate (k) is a product of the transmission coefficient and the frequency of attempts, a rate of 6.12 × 10^{-4} s^{-1} can be derived based on the experimentally observed frequency of about 2855 cm^{-1} for the C–H stretching vibration in the H-formyl group.[15]

$$P(E) = e^{-\pi^2 \omega \frac{\sqrt{2m(V_0 - E)}}{h}} \qquad \text{(Eq 1)}$$

By analogy, the tunneling probabilities for the conversion from the two nitrenes *syn*-^{3}**15** and *syn*-^{3}**16** to ketenes *syn*-^{3}**19** and *syn*-^{3}**20** have also been estimated by performing similar potential energy scans at the same theoretical level (Figure 5). The results suggest that both the barrier heights (V_0–E) of 20.8 (Figure S8) and 24.5 kcal mol^{-1} (Figure S9) and widths (w) of 3.10 and 3.48 Bohr in these two rearrangement reactions are larger than those in the nitrene ^{3}**2** → ketene ^{3}**3** conversion (Figure 5). As a result, the corresponding tunneling probabilities (P(E)) 4.16 × 10^{-24} and 3.27 × 10^{-29} are significantly smaller. Considering the experimentally observed C–H stretching frequencies of 2858.9 (*syn*-^{3}**15**) and 2864.1 cm^{-1} (*syn*-^{3}**16**), the rate constants are 3.57 × 10^{-10} and 2.81 × 10^{-15} s^{-1}, which are more than five orders of magnitude slower than that for the tunneling transformation of nitrene ^{3}**2**. Therefore, hydrogen-atom tunneling will be far too slow to be observable for nitrenes *syn*-^{3}**15** and *syn*-^{3}**16**.

CONCLUSIONS

The photochemistry of 3-azido-2-formylthiophene (**13**) and 3-azido-2-formylfuran (**14**) has been studied by combining matrix-isolation and quantum chemical calculations. Two new heteroaryl nitrenes, 3-nitrene-2-formylthiophene (**15**) and 3-nitrene-2-formylfuran (**16**), in two conformations with triplet ground state have been generated and characterized by using

matrix-isolation IR spectroscopy. In sharp contrast to the spontaneous hydrogen-atom tunneling of the structurally related 2-formyl phenylnitrene (**8**) to an imino ketene **9** in solid Ar-matrix at 10.0 K, the two conformers of nitrenes **15** and **16** are persistent in cryogenic Ar- and N_2-matrices up to 25.0 K due to higher activation barriers and the associated barrier heights for the 1,4-H migration. However, both nitrenes are photosensitive, and green-light irradiation (532 nm) results in cyclization to form 3,2-thienoisoxazole (**17**) and 3,2-furoisoxazole (**18**), respectively. In the gas phase, the thermal decomposition of the azide **13** mainly yields imino ketene in two conformations **19**/**19'**, which can be interconverted in matrices under selective irradiation conditions. Furthermore, the photoisomerization from isoxazole **17** to imino ketene **19** has also been observed. Whereas, pyrolysis of gaseous azide **14** results in complete fragmentation with traces of imino ketene **20**.

ASSOCIATED CONTENT

Supporting Information

Experimental band positions and calculated vibrational frequencies, calculated vertical transitions, energies and atomic coordinates for all species discussed in the paper. This material is available free of charge via the internet at http://pubs.acs.org.

AUTHOR INFORMATION

Corresponding Author

*X. Q. Zeng: E-mail, xqzeng@suda.edu.cn

Notes

The authors declare no competing financial interest.

ACKNOWLEDGMENTS

This work was supported by the National Natural Science Foundation of China (21673147). We thank Yan Lu for performing the CASPT2 calculations.

REFERENCES

(1) Lee, H.; Lee, J. K.; Min, S.-J.; Seo, H.; Lee, Y.; Rhee, H. Copper(I)-Catalyzed Synthesis of 1,4-Disubstituted 1,2,3-Triazoles from Azidoformates and Aryl Terminal Alkynes. *J. Org. Chem.* **2018**, *83*, 4805−4811.

(2) Carsch, K. M.; DiMucci, I. M.; Iovan, D. A.; Li, A.; Zheng, S.-L.; Titus, C. J.; Lee, S. J.; Irwin, K. D.; Nordlund, D.; Lancaster, K. M.; et al. Synthesis of a Copper-Supported Triplet Nitrene Complex Pertinent to Copper-Catalyzed Amination. *Science* **2019**, *365*, 1138−1143.

(3) Inokuma, Y.; Kawano, M.; Fujita, M. Crystalline Molecular Flasks. *Nat. Chem.* **2011**, *3*, 349–358.

(4) Sato, H.; Matsuda, R.; Sugimoto, K.; Takata, M.; Kitagawa, S. Photoactivation of a Nanoporous Crystal for On-Demand Guest Trapping and Conversion. *Nat. Mater.* **2010**, *9*, 661–666.

(5) Cheng, M.; Guo, C. Y.; Gross, M. L. The Application of Fluorine-Containing Reagents in Structural Proteomics. *Angew. Chem., Int. Ed.* **2020**, DOI: 10.1002/anie.201907662.

(6) Huisgen, R. Altes und Neues über aliphatische Diazoverbindungen. *Angew Chem.* **1955**, *67*, 439−463.

(7) Huisgen, R.; Vossius, D.; Appl, M. Die Thermolyse des Phenylazids in primären Aminen; die Konstitution des Dibenzamils. *Chem. Ber.* **1958**, *91*, 1−12.

(8) Huisgen, R.; Appl, M. Der Chemismus der Ringerweiterung beim Zerfall des Phenylazids in Anilin. *Chem. Ber.* **1958**, *91*, 12−21.

(9) Smolinsky, G.; Wasserman, E.; Yager, W. A. The E.P.R. of Ground State Triplet Nitrenes. *J. Am. Chem. Soc.* **1962**, *84*, 3220−3221.

(10) Gritsan, N. P.; Platz, M. S. Kinetics, Spectroscopy, and Computational Chemistry of Arylnitrenes. *Chem. Rev.* **2006**, *106*, 3844−3867.

(11) Mendez-Vega, E.; Mieres-Perez, J.; Chapyshev, S. V.; Sander, W. Persistent Organic High-Spin Trinitrenes. *Angew. Chem., Int. Ed.* **2019**, *58*, 12994−12998.

(12) Wentrup, C. Flash Vacuum Pyrolysis of Azides, Triazoles, and Tetrazoles. *Chem. Rev.* **2017**, *117*, 4562−4623.

(13) Borden, W. T.; Gritsan, N. P.; Hadad, C. M.; Karney, W. L.; Kemnitz, C. R.; Platz, M. S. The Interplay of Theory and Experiment in the Study of Phenylnitrene. *Acc. Chem. Res.* **2000**, *33*,

765−771.

(14) Kuzaj, M.; Lüerssen, H.; Wentrup, C. ESR Observation of Thermally Produced Triplet Nitrenes and Photochemically Produced Triplet Cycloheptatrienylidenes. *Angew. Chem., Int. Ed. Engl.* **1986**, *25*, 480−482.

(15) Nunes, C. M.; Knezz, S. N.; Reva, I.; Fausto, R.; McMahon, R. J. Evidence of a Nitrene Tunneling Reaction: Spontaneous Rearrangement of 2-Formyl Phenylnitrene to an Imino Ketene in Low-Temperature Matrixes. *J. Am. Chem. Soc.* **2016**, *138*, 15287−15290.

(16) Nunes, C. M.; Reva, I.; Kozuch, S.; McMahon, R. J.; Fausto, R. Photochemistry of 2-Formylphenylnitrene: A Doorway to Heavy-Atom Tunneling of a Benzazirine to a Cyclic Ketenimine. *J. Am. Chem. Soc.* **2017**, *139*, 17649−17659.

(17) Nunes, C. M.; Eckhardt, A. K.; Reva, I.; Fausto, R.; Schreiner, P. R. Competitive Nitrogen versus Carbon Tunneling. *J. Am. Chem. Soc.* **2019**, *141*, 14340−14348.

(18) Wentrup, C. Carbenes and Nitrenes: Recent Developments in Fundamental Chemistry. *Angew. Chem., Int. Ed.* **2018**, *57*, 11508–11521.

(19) Kvaskoff, D.; Bednarek, P.; George, L.; Waich, K.; Wentrup, C. Nitrenes, Diradicals, and Ylides. Ring Expansion and Ring Opening in 2-Quinazolylnitrenes. *J. Org. Chem.* **2006**, *71*, 4049−4058.

(20) Liu, Q.; Qin, Y. Y.; Lu, Y.; Wentrup, C.; Zeng, X. Q. Spectroscopic Characterization of Nicotinoyl and Isonicotinoyl Nitrenes and the Photointerconversion of 4-Pyridylnitrene with Diazacycloheptatetraene. *J. Phys. Chem. A* **2019**, *123*, 3793−3801.

(21) Liu, Q.; Wan, H. B.; Lu, Y.; Lu, B.; Zeng, X. Q. Photodecomposition of 1*H*-Pyrrole Carbonyl Azides: Direct Observation of Singlet 1*H*-Pyrrole Carbonyl Nitrenes and Triplet 1*H*-3-Pyrrylnitrene. *Eur. J. Org. Chem.* **2019**, *2019*, 401−411.

(22) Wentrup, C. Nitrenes, Carbenes, Diradicals, and Ylides. Interconversions of Reactive Intermediates. *Acc. Chem. Res.* **2011**, *44*, 393−404.

(23) Evans, R. A.; Wong, M. W.; Wentrup, C. 2-Pyridylnitrene−1,3-Diazacyclohepta-1,2,4,6-tetraene Rearrangements in the Trifluoromethyl-2-pyridyl Azide Series. *J. Am. Chem. Soc.* **1996**, *118*, 4009−4017.

(24) Wentrup, C.; Winter, H. W. Isolation of Diazacycloheptatetraenes from Thermal Nitrene-Nitrene Rearrangements. *J. Am. Chem. Soc.* **1980**, *102*, 6159−6161.

(25) Feng, R. J.; Lu, Y.; Deng, G. H.; Xu, J.; Wu, Z.; Li, H. M.; Liu, Q.; Kadowaki, N.; Abe, M.; Zeng, X. Q. Magnetically Bistable Nitrenes: Matrix Isolation of Furoylnitrenes in Both Singlet and Triplet States and Triplet 3-Furylnitrene. *J. Am. Chem. Soc.* **2018**, *140*, 10−13.

(26) Yang, Y.; Deng, G. H.; Lu, Y.; Liu, Q.; Abe, M.; Zeng, X. Q. Photodecomposition of Thienylsulfonyl Azides: Generation and Spectroscopic Characterization of Triplet Thienylsulfonyl Nitrenes and 3-Thienylnitrene. *J. Phys. Chem. A* **2019**, *123*, 9311−9320.

(27) Gronowitz, S.; Westerlund, C.; Hörnfeldt, A. B. The Synthetic Utility of Heteroaromatic Azido Compound. I. Preparation and Reduction of Some 3-Azido-2-substituted Furans, Thiophenes, and Selenophenes. *Acta Chem. Scand. Ser. B* **1975**, *29*, 224–232.

(28) Becke, A. D. Density-Functional Thermochemistry. III. The Role of Exact Exchange. *J. Chem. Phys.* **1993**, *98*, 5648−5652.

(29) Adamo, C.; Barone, V. Exchange Functionals with Improved Long-Range Behavior and Adiabatic Connection Methods without Adjustable Parameters: The mPW and mPW1PW Models. *J. Chem. Phys.* **1998**, *108*, 664−675.

(30) Zhao, Y.; Truhlar, D. G. The M06 Suite of Density Functionals for Main Group Thermochemistry, Thermochemical Kinetics, Noncovalent Interactions, Excited States, and Transition Elements: Two New Functionals and Systematic Testing of Four M06-Class Functionals and 12 other Functionals. *Theor. Chem. Acc.* **2008**, *120*, 215−241.

(31) Montgomery, J. A.; Frisch, M. J.; Ochterski, J. W.; Petersson, G. A. A Complete Basis Set Model Chemistry. VII. Use of the Minimum Population Localization Method. *J. Chem. Phys.* **2000**, *112*, 6532−6542.

(32) Watts, J. D.; Gauss, J.; Bartlett, R. J. Coupled-Cluster Methods with Noniterative Triple Excitations for Restricted Open-Shell Hartree-Fock and Other General Single Determinant Reference Functions. Energies and Analytical Gradients. *J. Chem. Phys.* **1993**, *98*, 8718−8733.

(33) Celani, P.; Werner, H.-J. Multireference Perturbation Theory for Large Restricted and Selected Active Space Reference Wave Functions. *J. Chem. Phys.* **2000**, *112*, 5546–5557.

(34) Stratmann, R. E.; Scuseria, G. E.; Frisch, M. J. An Efficient Implementation of Time-Dependent Density-Functional Theory for the Calculation of Excitation Energies of Large Molecules. *J. Chem. Phys.* **1998**, *109*, 8218−8224.

(35) Foresman, J. B.; Head-Gordon, M.; Pople, J. A.; Frisch, M. J. Toward a Systematic

Molecular Orbital Theory for Excited States. *J. Phys. Chem.* **1992**, *96*, 135−149.

(36) Gonzalez, C.; Schlegel, H. B. An Improved Algorithm for Reaction Path Following. *J. Chem. Phys.* **1989**, *90*, 2154−2161.

(37) Gonzalez, C.; Schlegel, H. B. Reaction Path Following in Mass-Weighted Internal Coordinates. *J. Phys. Chem.* **1990**, *94*, 5523−5527.

(38) Frisch, M. J.; Trucks, G. W.; Schlegel, H. B.; Scuseria, G. E.; Robb, M. A.; Cheeseman, J. R.; Scalmani, G.; Barone, V.; Mennucci, B.; Petersson, G. A.; et al. *Gaussian 09*, rev. E.01; Gaussian, Inc.: Wallingford, CT, 2013.

(39) Werner, H.-J.; Knowles, P. J.; Knizia, G.; Manby, F. R.; Schütz, M. Molpro: a General-Purpose Quantum Chemistry Program Package. *WIREs Comput. Mol. Sci.* **2012**, *2*, 242−253.

(40) Mieres-Perez, J.; Costa, P.; Mendez-Vega, E.; Crespo-Otero, R.; Sander, W. Switching the Spin State of Pentafluorophenylnitrene: Isolation of a Singlet Arylnitrene Complex. *J. Am. Chem. Soc.* **2018**, *140*, 17271−17277.

(41) Tsegaw, Y. A.; Kadam, P. E.; Tötsch, N.; Sanchez-Garcia, E.; Sander, W. Is Magnetic Bistability of Carbenes a General Phenomenon? Isolation of Simple Aryl(trifluoromethyl)carbenes in Both Their Singlet and Triplet States. *J. Am. Chem. Soc.* **2017**, *139*, 12310−12316.

(42) Merrick, J. P.; Moran, D.; Radom, L. An Evaluation of Harmonic Vibrational Frequency Scale Factors. *J. Phys. Chem. A* **2007**, *111*, 11683−11700.

(43) Deng, G. H.; Dong, X. L.; Liu, Q. F.; Li, D. Q.; Li, H. M.; Sun, Q.; Zeng, X. Q. The Decomposition of Benzenesulfonyl Azide: a Matrix Isolation and Computational Study. *Phys. Chem. Chem. Phys.* **2017**, *19*, 3792−3799.

(44) Hayes, J. C.; Sheridan, R. S. Infrared Spectrum of Triplet Phenylnitrene. On the Origin of Didehydroazepine in Low-Temperature Matrices. *J. Am. Chem. Soc*. **1990**, *112*, 5879−5881.

(45) Akai, N.; Kudoh, S.; Nakata, M. UV Photolysis of 1,4-Diaminobenzene in a Low-Temperature Argon Matrix to 2,5-Cyclohexadiene-1,4-diimine via 4-Aminoanilino Radical. *J. Phys. Chem. A* **2003**, *107*, 6725−6730.

(46) Gaywood, A. P.; McNab, H. Synthesis and Chemistry of 4,5-Dihydrothieno[3,2-*b*]pyrrol-6-one−A Heteroindoxyl. *J. Org. Chem.* **2009**, *74*, 4278−4282.

(47) Hrovat, D. A.; Waali, E. E.; Borden, W. T. Ab Initio Calculation of the Singlet-Triplet

Energy Difference in Phenylnitrene. *J. Am. Chem. Soc.* **1992**, *114*, 8698−8699.

(48) Borden, W. T. Reactions that Involve Tunneling by Carbon and the Role that Calculations have Played in Their Study. *WIREs Comput. Mol. Sci.* **2016**, *6*, 20−46.

TOC Graphic

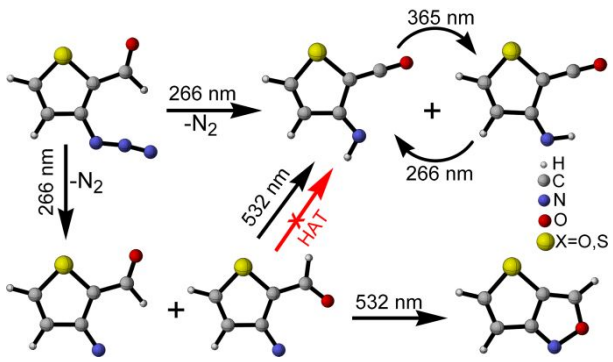

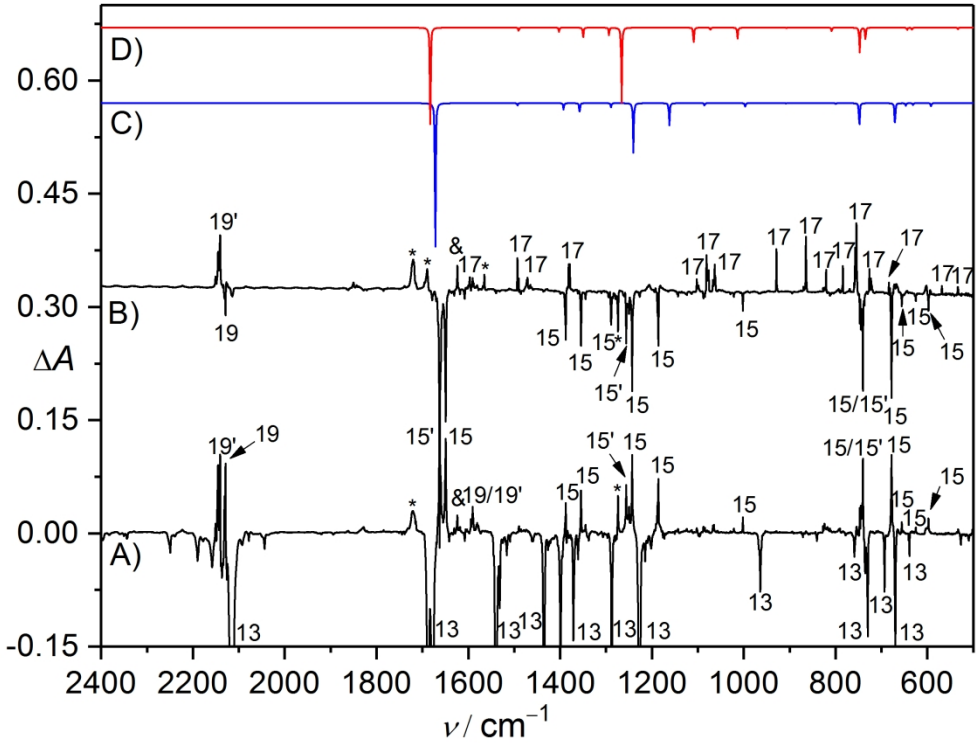

Figure 1. (A) IR difference spectrum showing the decomposition of 3-azido-2-formylthiophene (13) in Ar-matrix (10.0 K) upon 266 nm laser irradiation (11 s). (B) IR difference spectrum showing the rearrangement of nitrenes 15 (syn) and 15' (anti) to isoxazole 17 upon subsequent visible light irradiation (532 nm, 15 min). (C, D) B3LYP/6-311++G(3df,3pd) calculated IR spectra (scaled by a factor of 0.98) for nitrenes 15 (syn) and 15' (anti) in the triplet state. Bands of imino ketenes 19 (syn), 19' (anti), H2O (&), and unknown species (*) are also marked.

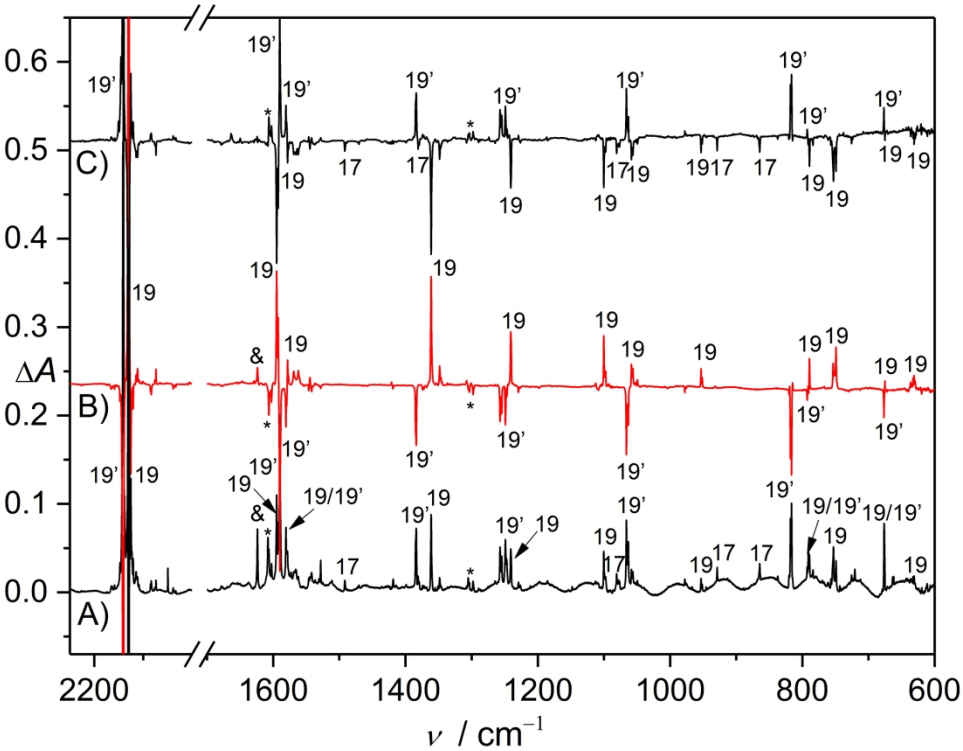

Figure 2. (A) Ar-matrix IR spectrum of the high-vacuum flash pyroysis (ca. 1000 K) products of 3-azido-2-formylthiophene (13). (B) IR difference spectrum showing rearrangement of imino ketenes 19' (anti) to 19 (syn) upon UV-light irradiation (365 nm, 25 min). (C) IR difference spectrum showing rearrangement of imino ketenes 19 (syn) to 19' (anti) upon 266 nm laser irradiation (2 min). Bands of isoxazole 17, H2O (&), and unknown species (*) are also marked.

227x172mm (300 x 300 DPI)

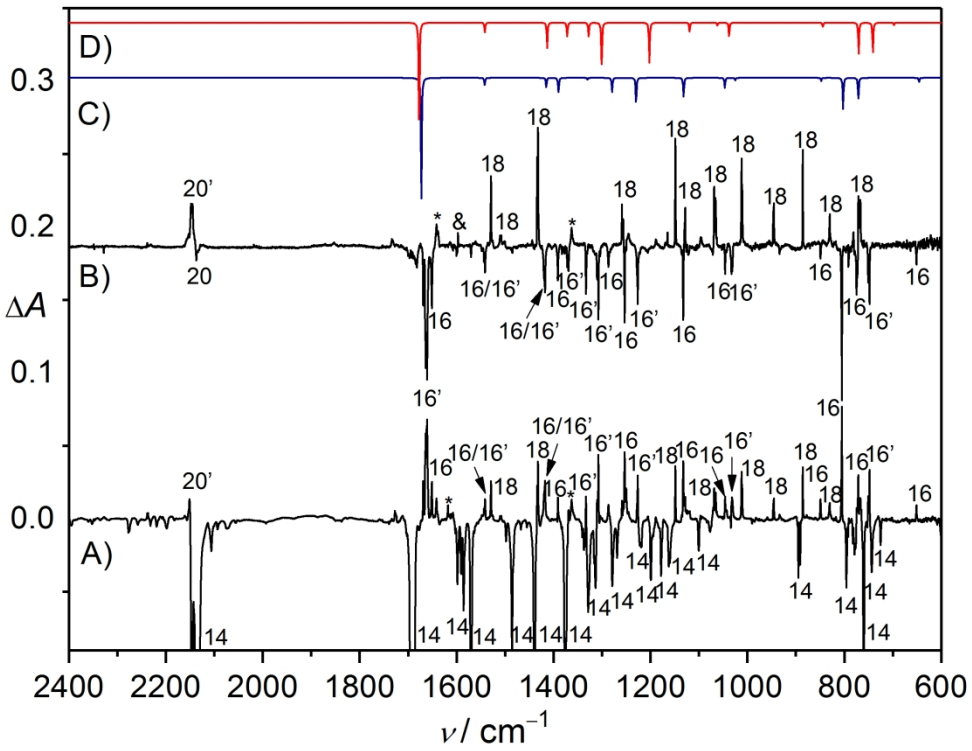

Figure 3. (A) IR difference spectrum showing the decomposition of 3-azido-2-formylfuran (14) in N2-matrix (15.0 K) upon 266 nm laser irradiation (55 s). (B) IR difference spectrum (3 times expanded along the ΔA axis) showing the rearrangement of nitrenes 16 and 16' to isoxazole 18 upon subsequent visible-light irradiation (532 nm, 55 min). (C, D) B3LYP/6-311++G(3df,3pd) calculated IR spectra (scaled by a factor of 0.98) for 16 (C: syn) and 16' (D: anti) in the triplet state. Bands of imino ketenes 20/20', H2O (&), and unknown species (*) are also marked.

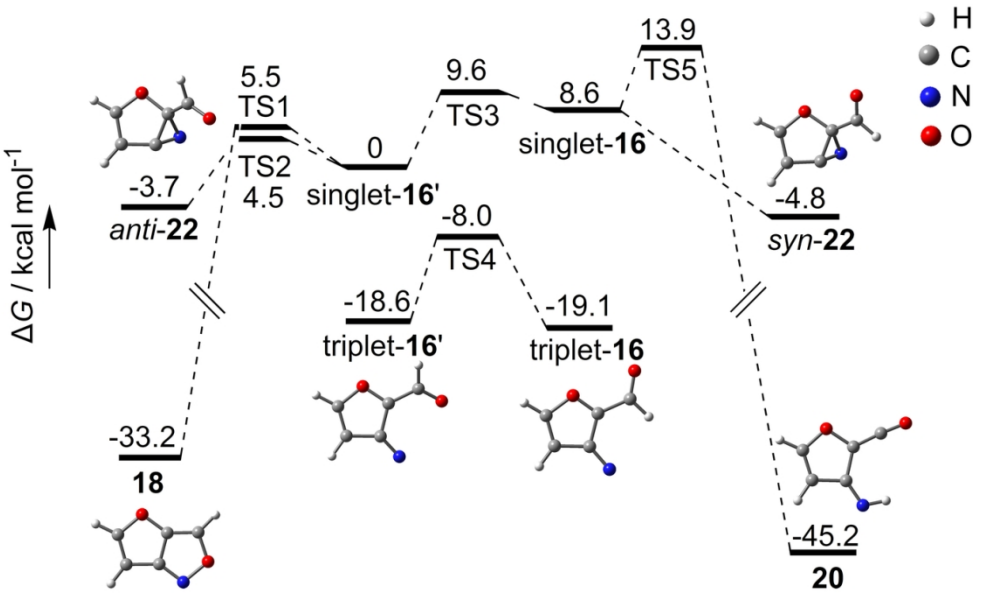

Figure 4. Calculated relative Gibbs free energy profile (kcal mol−1, including zero-point vibrational energy corrections) for the rearrangement of closed-shell singlet state 3-nitrene-2-formylfuran (16) at the CCSD(T)/aug-cc-pVTZ//B3LYP/6-311++G(3df,3pd) level.

119x73mm (300 x 300 DPI)

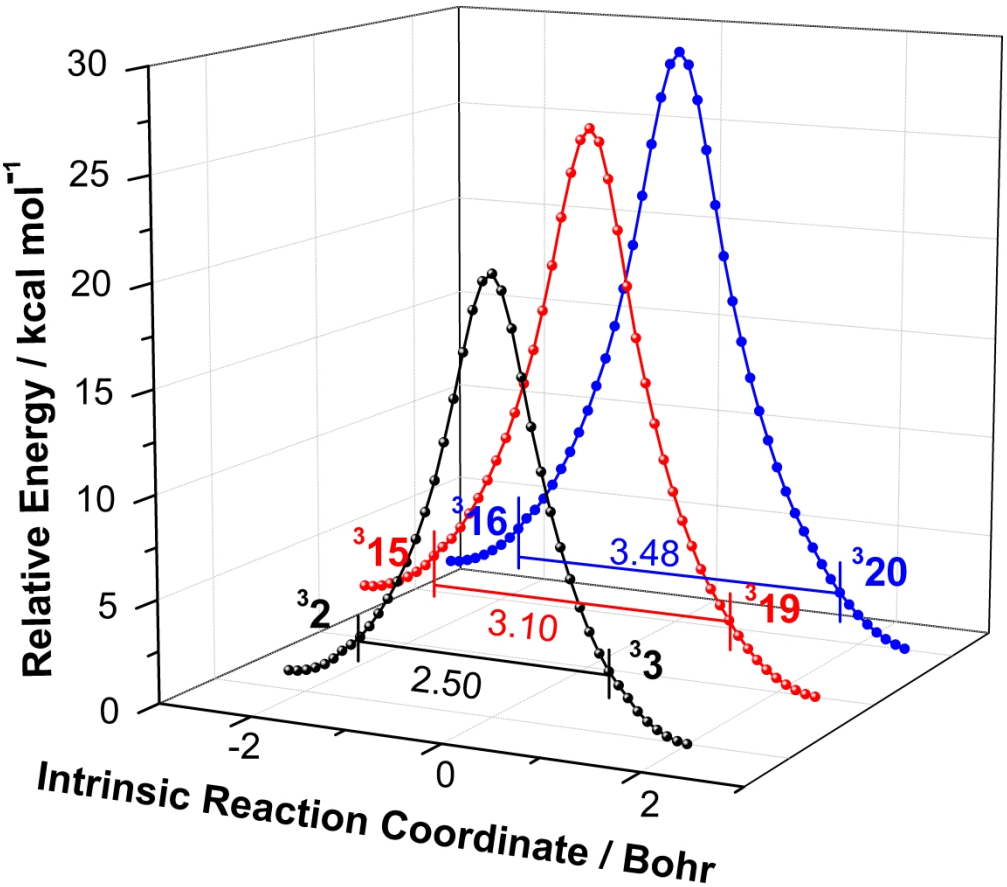

Figure 5. B3LYP/6-311++G(3df,3pd) calculated intrinsic reaction coordinate (IRC) profiles for rearrangement of triplet nitrenes (32, syn-315, and syn-316) to triplet ketenes (33, syn-319, and syn-320) via intramolecular 1,4-H shift. The estimated widths of the barriers (in Bohr) are also indicated.

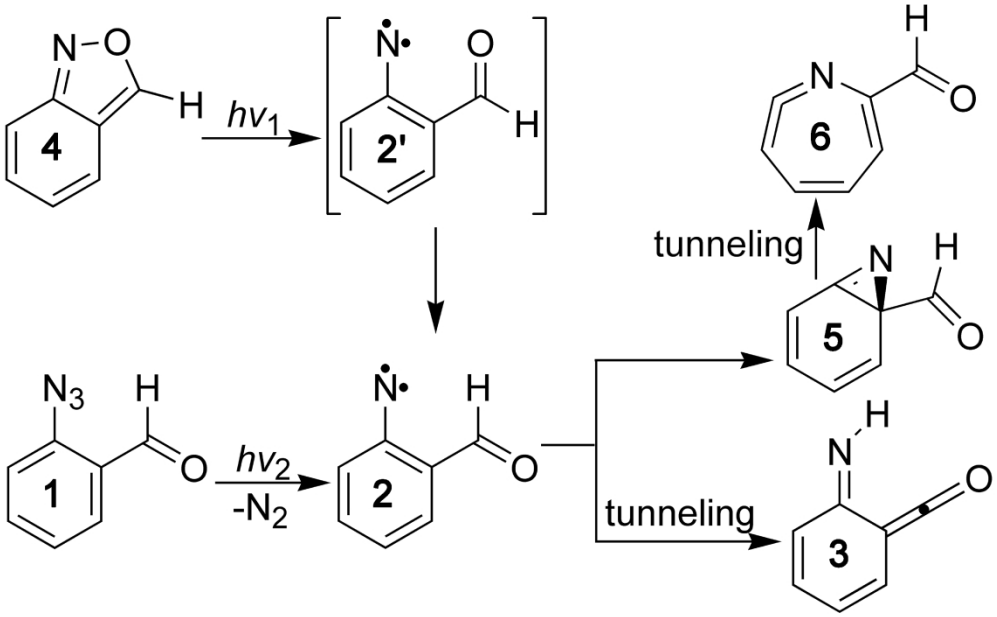

Scheme 1. The generation and isomerization of 2-formyl phenylnitrene (2).15,16

254x159mm (600 x 600 DPI)

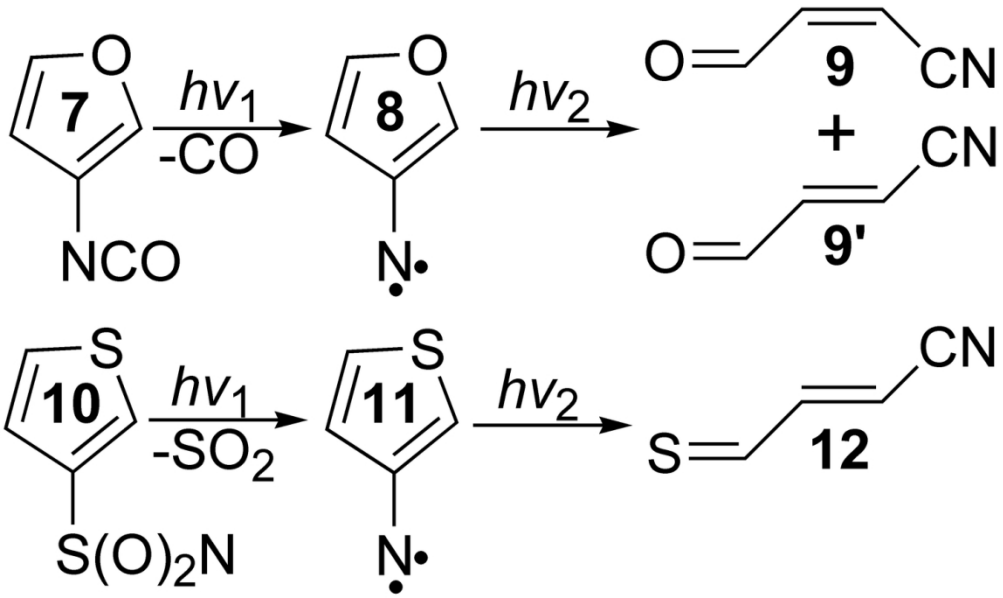

Scheme 2. The generation and isomerization of 3-furylnitrene (8)25 and 3-thienylnitrene (11).26

63x37mm (600 x 600 DPI)

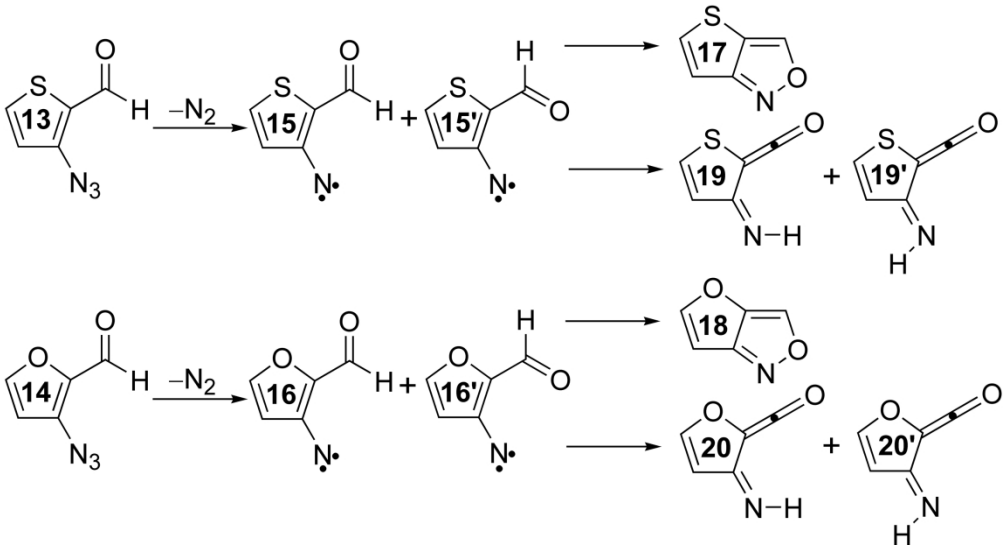

Scheme 3. Proposed photochemistry of 3-azido-2-formylthiophene (13) and 3-azido-2-formylfuran (14).

126x68mm (600 x 600 DPI)

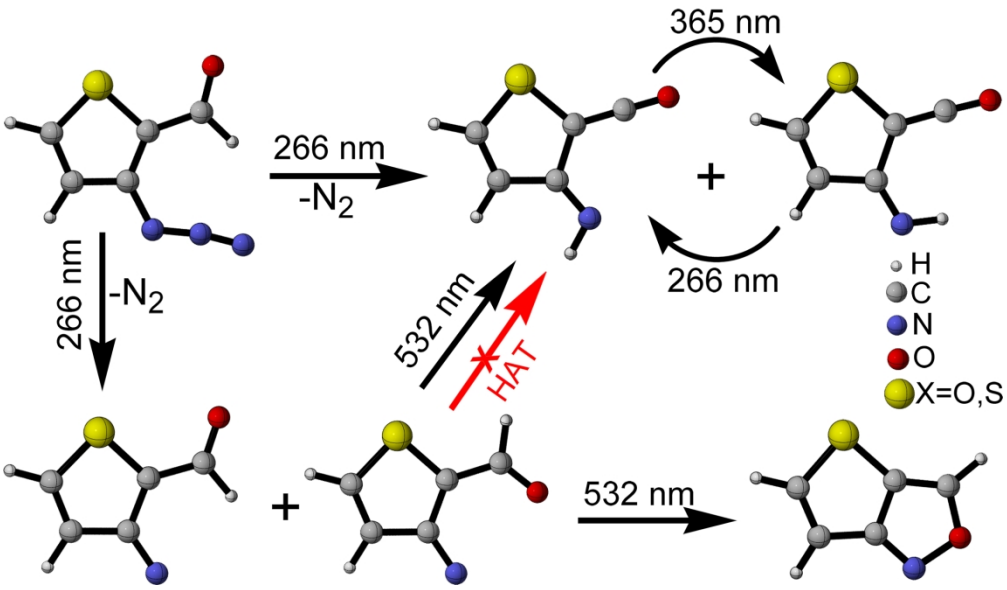

TOC Graphic

94x54mm (600 x 600 DPI)